RESEARCH ARTICLE

MHD Hybrid Nanofluid Flow with Heat Radiation over a Stretching Surface: Numerical Approach

Ahmad Taj[1,*], **Tanzila Ibrahim**[1,*], **Aqsa Murad**[1], **Ayesha Ali**[1] **and Saeed Islam**[1]

[1] Department of Mathematics, Abdul Wali Khan University Mardan, Khyber, Pakhtunkhwa 23200, Pakistan

Abstract

This study investigates the three-dimensional magnetohydrodynamic (MHD) radiative flow and heat transfer of a kerosene-based hybrid nanofluid containing Al_2O_3 and Cu nanoparticles over a stretching sheet. The governing partial differential equations (PDEs) are formulated and transformed into a coupled system of ordinary differential equations (ODEs) via suitable similarity transformations. The resulting nonlinear ODEs are solved using the Homotopy Analysis Method (HAM), with the effects of various physical parameters on velocity and temperature profiles illustrated through graphical and numerical results. Furthermore, the influences of key parameters—including skin friction coefficients, heat transfer characteristics, rotation parameter, Biot number, and magnetic field strength—on the flow and thermal behaviors are analyzed. The findings reveal that the rotation parameter, Biot number, and magnetic field strength significantly affect the velocity profiles and heat transfer performance of the hybrid nanofluid system.

Keywords: hybrid nanofluid, magnetohydrodynamics (MHD), heat radiation, stretching sheet, homotopy analysis method (HAM).

Special Symbols

Symbol	Description
ρ	Density
μ	Dynamic Viscosity
ν	Kinematic Viscosity
ξ	Transformed Coordinates
ϕ	Nanoparticle volume fraction
Ω	Transformed Angular Velocity
σ	Electrical Conductivity
ω	Angular Velocity
γ	Biot number

Subscripts

Symbol	Description
f	Fluid
bf	Base fluid
nf	Nanofluid
hnf	Hybrid Nanofluid

Submitted: 08 July 2025
Accepted: 11 August 2025
Published: 19 March 2026

Vol. 2, **No.** 1, 2026.
10.62762/IJTSSE.2025.263639

***Corresponding authors:**
✉ Ahmad Taj
ahmadtaj843@gmail.com
✉ Tanzila Ibrahim
tanzeelaibrahimawkum@gmail.com

Citation
Taj, A., Ibrahim, T., Murad, A., Ali, A., & Islam, S. (2026). MHD Hybrid Nanofluid Flow with Heat Radiation over a Stretching Surface: Numerical Approach. *International Journal of Thermo-Fluid Systems and Sustainable Energy*, 2(1), 4–17.

List of Symbols

Symbol	Description
T	Temperature
u, v, w	Velocity components
h	Heat transfer coefficient
f, g	Dimensionless velocities
θ	Dimensionless temperature
s	Shape factor
Nu	Nusselt number
k	Thermal Conductivity
Re	Reynolds number
C_p	Specific Heat
R_d	Radiation parameter
τ_{xy}	Shear stress

1 Introduction

A fluid with nanoparticles, particles with sizes in the nanometer range dispersed throughout a base fluid, is called a nanofluid. As the nanoparticles are evenly dispersed throughout the fluid medium, these fluids are essentially colloidal suspensions [1, 2]. Usually found in nanofluids, nanoparticles are composed of metals, metal oxides, carbides, or carbon nanotubes. Water, ethylene glycol, and different types of oil are frequently used as base fluids for these solutions [3].

Nanofluids have a wide range of uses in heat transfer processes, including fuel cells, microelectronics, engine cooling systems, vehicle thermal management, home refrigeration, chillers, heat exchangers, and boiler flue gas grinding, machining, and temperature reduction [4, 5]. Nanofluids have improved convective heat transfer and thermal conductivity when compared to their respective base fluids [6]. Understanding the rheological characteristics of nanofluids is essential for determining their suitability for convective heat transfer applications [7, 8].

When exposed to ultrasonic fields, nanofluids exhibit shear-wave reconversion from incident compressional waves in addition to their unique acoustic characteristics; this effect increases with increasing concentrations of nanoparticles [9]. In simulations of computational fluid dynamics (CFD), nanofluids are frequently handled as single-phase fluids [10, 11]. Nevertheless, a two-phase assumption is used in practically all scholarly works. Classical single-phase fluid theory states that the concentrations and features of a nanofluid's constituent parts determine its physical characteristics [12]. A different approach is to use a two-phase or two-component framework to model nanofluids [13].

By promoting the dispersion of a nanofluid droplet and creating a structural disjoining pressure close to the contact line, the nanoparticles use diffusion to build a solid-like ordered structure along the contact line [14]. This improvement is not seen, though, for droplets with diameters in the nanometer range since the wetting time scale is substantially shorter than the diffusion time scale [15].

Heat transfer rate is a key factor in many industrial processes' qualitative output. Water and ethylene glycol are examples of common fluids with a restricted potential for heat transmission. To improve the basic fluids thermal characteristics, researchers began incorporating nanoparticles into them. Thus, nanofluids are defined as the suspension of unchanging, uniformly dispersed nanoparticles in base fluids, such as methanol, ethylene glycol, and water (H_2O). Each nanofluid has unique properties that depend on the base fluid and these microscopic particles. Metals, metal oxides such as Cu, Ag, SiO_2, TiO_2, Fe_2O_3, and carbon nanotubes (MWCNTs and SWCNTs) are among the materials that make up these nanoparticles. The nanoparticles floating in these fluids have an average diameter that is with an average diameter ranging from 1 to 100 nanometers (nm).

The limited thermal conductivity of common base fluids, such as water and ethylene, limits their use in many real-world applications. A new class of fluids known as nanofluids was created to get around this restriction by adding different kinds of nanoparticles to improve their thermal characteristics [16]. Nanofluids are extensively utilized in a wide range of industrial and engineering applications, including solar collectors, microchannel heat sinks, refrigeration systems, electronic device cooling, HVAC systems, and even the food sector, because of their exceptional heat transfer capabilities [17–19]. Research on using nanofluids to improve heat transfer has rapidly expanded during the last ten years.

Although conventional fluids like water and air are commonly used as cooling media, the rate of heat exchange that these fluids can achieve is unsuitable for some sheet materials. For this reason, the use of magnetic fields seems to be acceptable due to its simplicity and non-intrusiveness. Solar collectors are devices that efficiently and sustainably transform solar energy into thermal energy. To increase their capacity to transform the necessary form of energy, these solar

collectors employ a variety of nanofluid types. The use of nanofluids to improve the thermal performance of solar collectors has been the subject of numerous experimental and computational investigations.

2 Related Work

By suspending a variety of distinct nanoparticles in a base fluid, researchers created a novel type of nanofluid. Choi et al. [20] were the first to experimentally introduce the idea of nanofluids. In 1995, they found that, in contrast to traditional base fluids, nanofluids improved thermal efficiency. Subsequently, Kang et al. [21] verified these findings experimentally. Afterwards, Lee et al. [22] and Eastman et al. [23] evaluated the thermal conductivity of a water-based nanofluid containing aluminum oxide (Al_2O_3) and copper (Cu) nanoparticles. Nanofluids' heat transfer performance is greatly improved by their obvious increase in thermal conductivity when compared to conventional base fluids.

Based on the idea of their thermal conductivity, a variety of flow models, as well as the procedures and uses of hybrid nanofluids, have been studied [24]. Between two parallel disks, Ahmed et al. [25] examined the behavior of a nanofluid with Al_2O_3 nanoparticles in terms of squeezing flow. Furthermore, heat transmission and skin friction numerical and analytical results were emphasized. In their experimental study of the variation of the heat transfer rate for nanofluid (Fe_3O_4/H_2O) inside horizontal circular tubes under the effect of magnetic fields, Sun et al. [26] found that the intensity of the magnetic field and the heat transfer rate were directly correlated.

Kumar et al. [27] found that the use of nanofluids improved the reliability of electronic chips by 70% and reduced temperature, thermal resistance, and power consumption in a numerical comparison of heat transfer performance between conventional fluids and Al_2O_3/H_2O nanofluid systems. Under the influence of an applied magnetic field, Lahmar et al. [28] examined the thermal conductivity and heat transfer rate of (Fe_3O_4/H_2O) nanofluids trapped between two parallel plates. Sheikholeslami and Rokni [29] numerically studied the influence of Coulomb force on nanofluid heat transfer within a porous enclosure, considering thermal radiation effects. The magnetohydrodynamic (MHD) flow of a Casson nanofluid across a vertically positioned plate with convective heating and velocity slip effects was covered by Gbadeyan et al. [30]. Additionally, both numerical and graphical analyses are performed to examine the impact of radiation phenomena and heat conductivity on the flow.

A new category of nanofluids known as hybrid nanofluids is produced by mixing two or more different kinds of nanoparticles, either in a mixed or compound form. This method's main goal is to maximize the physical and chemical characteristics of various materials in order to create a special fluid with exceptional qualities. These artificial hybrid materials have remarkable qualities that none of the constituent parts could provide on their own. The creation, categorization, and use of diverse nanofluids have been the focus of a substantial amount of research. Performance evaluations of hybrid nanofluids, a new and inventive class of fluid, are now underway. The performance of nanofluids and hybrid nanofluids has been compared in a small number of recent studies [31–34].

An advanced kind of nanofluid called a hybrid or composite nanofluid is created when two or more metals, metal oxides, or a combination of the two are dissolved in a base fluid. The study of how magnetic fields interact with conducting fluids is known as magnetohydrodynamics, or MHD. When a fluid is moving and electrically conductive, currents are induced in reaction to magnetic fields, causing this phenomenon. The magnetic field itself is altered by the forces created by these induced currents acting on the fluid. The Navier-Stokes equations, which describe fluid dynamics, and Maxwell's equations, which explain the behavior of electromagnetic fields, combine to form the governing equations for MHD. The complete MHD phenomenon is captured by a collection of connected differential equations that are formed by these.

Kashi'ie et al. [35] investigated the fluidic system dynamics and heat transfer processes, taking into account the impacts of Joule heating, by computationally analyzing the MHD flow of a hybrid nanofluid (Al_2O_3/H_2O) due to a stretched sheet. Wole-Osho et al. [36] identified the hybrid nanofluid's (Al_2O_3-Zn/H_2O) flow characteristics and found that the concentration of nanoparticles had a major impact on the flow's viscosity and specific heat. Aly et al. [37] used both theoretical and computational methods to study the MHD stagnation point flow across a stretching sheet of hybrid nanofluid while taking slip and dissipation effects into account. They discovered a relationship between the heat transfer rate and MHD.

After analyzing the rheological performance of

tungsten oxide–engine oil nanofluid at different concentrations and temperatures, Aghahadi et al. [38] found a linear relationship between applied shear stress and shear rate. The Homotopy Analysis Method (HAM) was used by Hayat et al. [39] to study the MHD flow of a hybrid nanofluid (Al_2O_3–Cu/H_2O) across a revolving stretching sheet. Their research quantitatively examined the effects of different physical parameters on the system's temperature and velocity fields. The results offer important new information about the flow and temperature characteristics of hybrid nanofluids in rotating frames. Huminic et al. [40, 41] examined the rate of heat transfer and entropy creation for both traditional and hybrid nanofluids in a variety of physical settings.

A numerical study of the heat transfer behavior of a hybrid nanofluid passing through an asymmetric channel with porous walls was also carried out by Saba et al. [42]. Additionally, their work used graphical representations to show a variety of important physical impacts. To create hybrid nanoparticles (Di–Ag), de Oliveira et al. [43] carried out an experimental investigation on a unique technique for coating diamond nanoparticles with silver. In a second work, Iqbal et al. [44] examined how the Hall current affected the MHD flow of a hybrid nanofluid in a rotating channel while taking heat radiation and various nanoparticle morphologies into account. The mechanics of heat transmission in nanofluid flows has recently been the subject of numerous investigations [45–53].

Three elements make up the phrase magnetohydrodynamics: dynamics (signaling motion), hydro (signaling fluid, especially water), and magneto (signaling magnetic fields). Hannes Alfvén, who won the 1970 Nobel Prize in Physics for his groundbreaking contributions to the subject, set the groundwork for magnetohydrodynamics (MHD) [54]. These waves were first described by Alfvén as "electromagnetic–hydrodynamic waves." He did, however, propose a more straightforward nomenclature in a subsequent paper, writing: "It may be convenient to call this phenomenon 'magneto-hydrodynamic' waves, as the term 'electromagnetic–hydrodynamic waves' is somewhat complicated" [55].

The core, which is located beneath the Earth's mantle, is made up of a liquid outer core and a solid inner core that are both abundant in iron [56, 57]. The Coriolis effect causes swirling motions, or eddies, to emerge as the liquid outer core flows in the presence of Earth's magnetic field [58]. The geomagnetic dynamo, a self-sustaining process in which fluid motion produces magnetic fields that strengthen the planet's initial magnetic field, is aided by these eddies [59].

The electromagnetic radiation that matter emits due to the thermal motion of its constituent particles is referred to as thermal radiation. Thermal radiation is released by any material that has a temperature higher than absolute zero. Numerous internal processes, such as electrical excitations, molecular vibrations, and lattice oscillations within the material, are the source of the energy emitted [60]. Charge-acceleration or dipole oscillation transforms kinetic energy into electromagnetism. The majority of thermal radiation at ambient temperature is released in the infrared (IR) spectrum [61]. However, a significant amount of the radiation moves into the visible spectrum as the temperature rises above around 525 °C (977 °F), which results in the material emitting visible light. This phenomenon is called incandescence.

One of the basic processes of heat transport, in addition to conduction and convection, is thermal radiation. Thermal radiation is the main way that heat is transferred from the Sun to the Earth. The sky appears to be blue because of the partial absorption and dispersion of this energy in the atmosphere [62]. The atmosphere carries a large portion of the Sun's radiation to the surface, where it is either reflected or absorbed. Things or occurrences that are normally invisible to the human eye can be detected thanks to thermal radiation. This idea is used by thermographic cameras, which use infrared radiation to create thermal images that show temperature differences between surfaces. These pictures can show a scene's temperature gradient and are frequently used to find objects that are hotter than their surroundings. Animals and humans can be located using infrared imaging because of their body temperature in a dark setting with low levels of visible light. Another type of thermal radiation is cosmic microwave background radiation.

Thermal radiation in idealized systems is studied using the blackbody radiation concept. When a radiating object displays the properties of a perfect black body, this theoretical paradigm is applicable in thermodynamic equilibrium [63]. Planck's law links the body's temperature to its radiative energy production and characterizes the spectral distribution

of blackbody radiation. The Wien's displacement law establishes the wavelength (or frequency) at which a black body's radiation is most intense, whereas the Stefan-Boltzmann law controls the total radiant intensity released by the body [64]. In situations when blackbody radiation is not a reliable approximation, quantum electrodynamics (QED) can be used to represent emission and absorption [65].

One type of electromagnetic radiation that a material emits due to its temperature is called thermal radiation. A semi-analytical method for resolving nonlinear ordinary and partial differential equations is the Homotopy Analysis Method (HAM). It uses the topological idea of homotopy to produce a convergent series solution for nonlinear systems. This is accomplished by employing a homotopy-Maclaurin series to handle the system's nonlinearities. In his PhD dissertation [66], Liao Shijun of Shanghai Jiaotong University originally proposed the HAM in 1992. It was improved upon in 1997 to create a broader form of the homotopy for differential systems. As part of this adjustment, a non-zero auxiliary parameter called the convergence-control parameter was added [67, 68].

3 Problem statement

The three-dimensional flow of a hybrid nanofluid across a rotating and stretching surface is examined in this work. The surface stretches in the xy-plane, and the nanofluid travels in the positive z-direction ($z > 0$). u, v, and w stand for the velocity components in the x, y, and z directions, respectively. T_f and T denote the fluid's temperature and the surface temperature, respectively. The fluid-surface thermal interaction is described by a heat transfer coefficient, h_f. Furthermore, as shown in Figure 1, a uniform magnetic field B_0 is applied along the z-axis.

The following is an expression of the governing equations for energy balance, momentum, and mass conservation:

$$\frac{\partial u}{\partial x} + \frac{\partial v}{\partial y} + \frac{\partial w}{\partial z} = 0 \tag{1}$$

$$\begin{aligned}&\left[u\frac{\partial u}{\partial x} + v\frac{\partial u}{\partial y} + w\frac{\partial u}{\partial z} - 2\omega w\right]\\ &= \left(1 + \frac{1}{\lambda}\right)\frac{\mu_{\text{hnf}}}{\rho_{\text{hnf}}}\left[\frac{\partial^2 u}{\partial z} - \sigma_{\text{hnf}}B_0^2 u\right],\end{aligned} \tag{2}$$

$$\begin{aligned}&\left[u\frac{\partial v}{\partial x} + v\frac{\partial v}{\partial y} + w\frac{\partial v}{\partial z} - 2\omega u\right]\\ &= \left(1 + \frac{1}{\lambda}\right)\frac{\mu_{\text{hnf}}}{\rho_{\text{hnf}}}\left[\frac{\partial^2 v}{\partial z^2} - \sigma_{\text{hnf}}B_0^2 v\right],\end{aligned} \tag{3}$$

$$\begin{aligned}&(\rho C_p)_{\text{hnf}}\left[u\frac{\partial T}{\partial x} + v\frac{\partial T}{\partial y} + w\frac{\partial T}{\partial z}\right]\\ &= \left(K_{\text{hnf}} + \frac{16}{3}\frac{\sigma^* T_\infty^3}{k^*}\right)\frac{\partial^2 T}{\partial z^2}\\ &+ \mu_{\text{hnf}}\left(1 + \frac{1}{\lambda}\right)\left[\left(\frac{\partial u}{\partial z}\right)^2 + \left(\frac{\partial v}{\partial z}\right)^2\right],\end{aligned} \tag{4}$$

The boundary conditions are:

$$u = u_w = bx, \quad v = 0, \tag{5}$$

$$-K_{\text{hnf}}\left(\frac{\partial T}{\partial z}\right) = h_f\left(T_f - T\right) \quad \text{at } z = 0,$$

$$u \to 0, \quad v \to 0, \quad T \to T_\infty \quad \text{as } z \to \infty. \tag{6}$$

The hybrid nanofluid in question is made up of copper (Cu) and aluminum oxide (Al_2O_3) nanoparticles mixed and dissolved in kerosene. ϕ_1 and ϕ_2 represent the volume fractions of Al_2O_3 and Cu nanoparticles, respectively. The sum of $\phi_1 + \phi_2$ yields the overall concentration of nanoparticles in the hybrid nanofluid, ϕ_{hnf}. Table 1 lists the thermophysical characteristics of nanoparticles, including density, specific heat, and thermal conductivity. Table 2 lists the thermophysical properties of hybrid nanofluid, including viscosity, specific heat capacity, density, thermal conductivity, and electrical conductivity. ρ_f, ρ_{s1}, and ρ_{s2}, respectively, denote the densities of the base fluid, Al_2O_3, and Cu nanoparticles. $(C_p)_f$, $(C_p)_{\text{hnf}}$, $(C_p)_{s1}$ and $(C_p)_{s2}$ represent the specific heat capacities of the base fluid, the hybrid nanofluid, and the Al_2O_3 and Cu particles, respectively.

The following are the dimensional expressions for the Nusselt number and the skin friction coefficients:

$$\begin{aligned}C_f &= \frac{\mu_{\text{hnf}}}{\rho_f u_w^2}\left(\frac{\partial u}{\partial z}\right)_{z=0},\\ C_g &= \frac{\mu_{\text{hnf}}}{\rho_f u_w^2}\left(\frac{\partial v}{\partial z}\right)_{z=0},\\ Nu &= -\frac{xK_{\text{hnf}}}{k_f(T_f - T_\infty)}\left(\frac{\partial T}{\partial z}\right)_{z=0}.\end{aligned} \tag{7}$$

The following similarity transformations are used to reduce the system of partial differential equations

Table 1. Mathematical values of various properties for nanoparticles and base fluid.

Properties	Base fluid	Nano particles	
	Kerosene	Cu	Al_2O_3
Density (ρ) ($kg\,m^{-3}$)	783	8933	3970
Thermal conductivity (K) ($W\,m^{-1}\,K^{-1}$)	0.145	400	40
Specific heat (C_p) ($J\,kg^{-1}\,K^{-1}$)	2090	385	765

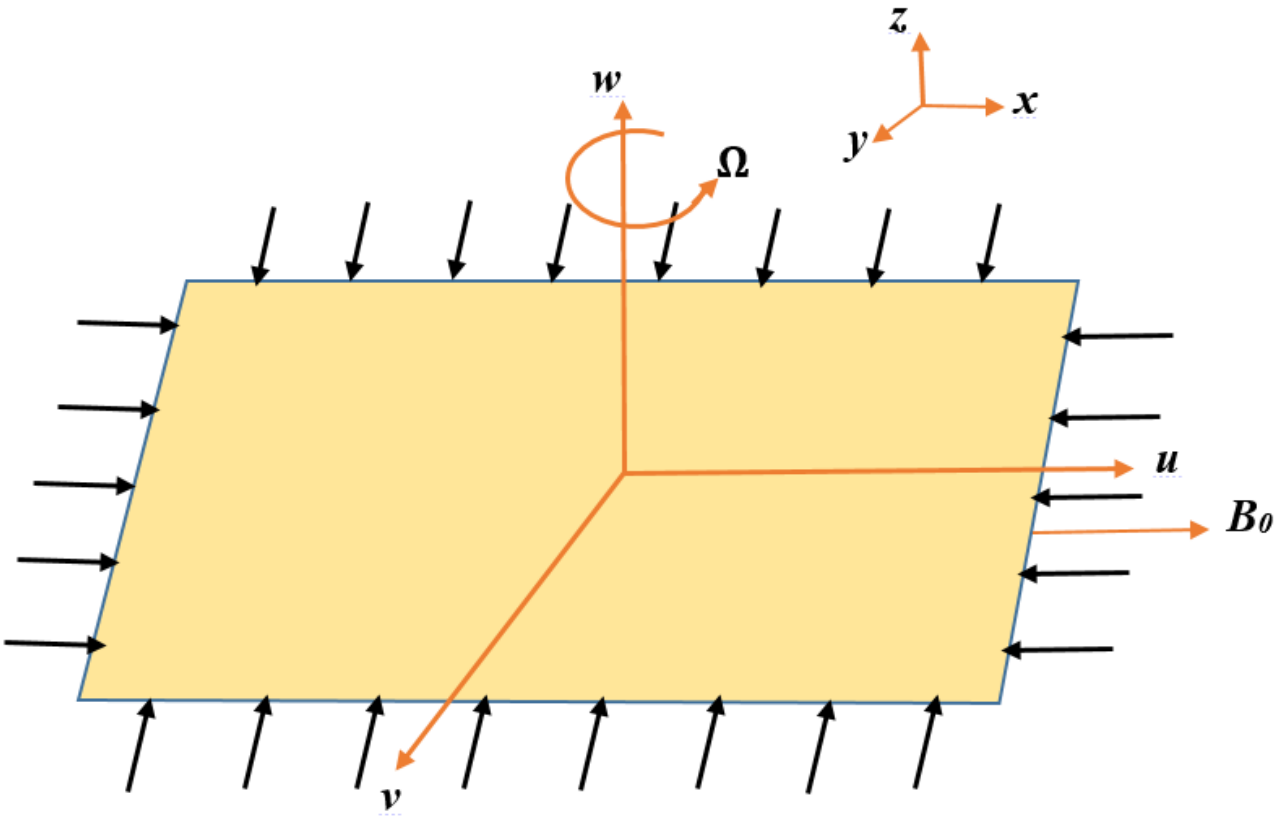

Figure 1. Geometrical representation of the problem.

(1-4) to a dimensionless set of ordinary differential equations:

$$u = bxf'(\xi), \quad v = bxg(\xi), \quad w = -\sqrt{b\nu_f}f(\xi),$$
$$\xi = \sqrt{\frac{b}{\nu_f}}z, \quad \theta(\xi) = \frac{T - T_\infty}{T_f - T_\infty}. \tag{8}$$

The system of equations (1-4) is changed into the following form by utilizing the previously established similarity transformations, which also automatically satisfy the continuity equation:

$$\left(1 + \frac{1}{\beta}\right) f''' - \frac{A_2}{A_1}\left[f'^2 - ff'' - 2\Omega g + A_3 M f'\right] = 0, \tag{9}$$

$$\left(1 + \frac{1}{\beta}\right) g'' - \frac{A_2}{A_1}\left[f'g - fg' - 2\Omega f' + A_3 M g\right] = 0, \tag{10}$$

$$\left[A_4 + R_d\right]\theta'' + A_5 Pr f\theta' + \left(1 + \frac{1}{\beta}\right) A_6 Ec\left(f''^2 + g'^2\right) = 0 \tag{11}$$

where,

$$A_1 = \frac{\mu_{\text{hnf}}}{\mu_f}, \quad A_2 = \frac{\rho_{\text{hnf}}}{\rho_f}, \quad A_3 = \frac{\sigma_{\text{hnf}}}{\sigma_f},$$
$$A_4 = \frac{k_{\text{hnf}}}{k_f}, \quad A_5 = \frac{(\rho C_p)_{\text{hnf}}}{(\rho C_p)_f} \tag{12}$$

Table 2. Thermophysical properties of hybrid nanofluid.

Properties	Hybrid nanofluid
Viscosity μ_{hnf}	$\frac{\mu_{\text{hnf}}}{\mu_f} = \frac{1}{[(1-\phi_1)(1-\phi_2)]^{\frac{5}{2}}}$
Specific heat capacity C_p	$[\rho C_p]_{\text{hnf}} = \left[(1-\phi_1) + \frac{(\rho C_p)_{s1}}{(\rho C_p)_f}\phi_1\right](1-\phi_2) + \phi_2\frac{(\rho C_p)_{s2}}{(\rho C_p)_f}$
Density ρ_{hnf}	$\frac{\rho_{\text{hnf}}}{\rho_f} = \left[\left(\frac{\rho_{s1}}{\rho_f}\right)\phi_1 + (1-\phi_1)\right](1-\phi_2) + \phi_2\frac{\rho_{s2}}{\rho_f}$
Thermal conductivity k_{hnf}	$\frac{k_{\text{hnf}}}{k_{\text{bf}}} = \frac{k_{s2} + k_{\text{bf}}(s-1) - (k_{\text{bf}} - k_{s2})(s-1)\phi_2}{(k_{\text{bf}} - k_{s2})\phi_2 + (s-1)k_{\text{bf}} + k_{s2}}$ $\frac{k_{\text{bf}}}{k_f} = \frac{k_{s1} + k_f(s-1) - (k_f - k_{s1})(s-1)\phi_1}{(k_f - k_{s1})\phi_1 + (s-1)k_f + k_{s1}}$
Electrical conductivity σ_{hnf}	$\frac{\sigma_{\text{hnf}}}{\sigma_{\text{bf}}} = \frac{\sigma_{s2} + 2\sigma_{\text{bf}} - 2(\sigma_{\text{bf}} - \sigma_{s2})\phi_2}{2\sigma_{\text{bf}} + \sigma_{s2} + (\sigma_{\text{bf}} - \sigma_{s2})\phi_2}$ $\frac{\sigma_{\text{bf}}}{\sigma_f} = \frac{2\sigma_f + \sigma_{s1} - 2(\sigma_f - \sigma_{s1})\phi_1}{2\sigma_f + \sigma_{s1} + (\sigma_f - \sigma_{s1})\phi_1}$

The boundary conditions are:

$$\begin{aligned} &f(\xi) = 0, \quad g(\xi) = 0, \quad f'(\xi) = 1, \\ &\theta'(\xi) = -\frac{k_f}{k_{\text{hnf}}}\gamma\left(1 - \theta(\xi)\right), \quad \text{at } \xi = 0, \end{aligned} \tag{13}$$

$$f'(\xi) \to 0, \quad g(\xi) \to 0, \quad \theta(\xi) \to 0, \quad \text{as } \xi \to \infty. \tag{14}$$

Dimensionless parameters involved in equations (9-11) can be written as:

$$\begin{aligned} &\Omega = \frac{\omega}{b}, \quad M = \frac{\sigma_f B_0^2}{b\rho_f}, \quad Pr = \frac{\mu_f (C_p)_f}{k_f}, \\ &R_d = \frac{16\sigma^* T_\infty^3}{3k^* k_f}, \quad Ec = \frac{b^2 x^2}{(C_p)_f (T_f - T_\infty)}, \quad \gamma = \frac{h_f}{k_f}\sqrt{\frac{\nu_f}{b}}. \end{aligned} \tag{15}$$

Equation (11), which provides the formulas for the skin friction coefficients and the Nusselt number, can be expressed as follows:

$$\begin{aligned} C_f r^{1/2} &= \frac{1}{(1-\phi_1)^{5/2}(1-\phi_2)^{5/2}} f''(0), \\ C_g r^{1/2} &= \frac{1}{(1-\phi_1)^{5/2}(1-\phi_2)^{5/2}} g'(0), \\ Nur^{-1/2} &= -\frac{k_{\text{hnf}}}{k_f}\theta'(0). \end{aligned} \tag{16}$$

where

$$r = \frac{u_w x}{\nu_f}. \tag{17}$$

4 Solution with HAM Method

The Homotopy Analysis Method (HAM), which is incorporated into Mathematica software, is used to numerically solve the transformed system of nonlinear ordinary differential equations, which is shown in Eqs.

(9-11). The final solution is given by the series at $q = 1$:

$$\begin{aligned} f(\xi) &= f_0(\xi) + f_1(\xi) + f_2(\xi) + \ldots, \\ g(\xi) &= g_0(\xi) + g_1(\xi) + g_2(\xi) + \ldots, \\ \theta(\xi) &= \theta_0(\xi) + \theta_1(\xi) + \theta_2(\xi) + \ldots \end{aligned} \tag{18}$$

OR

$$\begin{aligned} f(\xi) &= f_0(\xi) + \sum_{m=1}^{\infty} f_m(\xi), \\ g(\xi) &= g_0(\xi) + \sum_{m=1}^{\infty} g_m(\xi), \\ \theta(\xi) &= \theta_0(\xi) + \sum_{m=1}^{\infty} \theta_m(\xi). \end{aligned} \tag{19}$$

$\hbar_f, \hbar_g, \hbar_\theta$ are the auxiliary parameters that control the convergence of the series solutions. These parameters are usually chosen to guarantee both quick and steady convergence of the solution, frequently using graphical analysis employing so-called $\hbar$-curves.

5 Result and Discussions

In this section, we discussed the effect of various physical parameters on velocity and temperature profile.

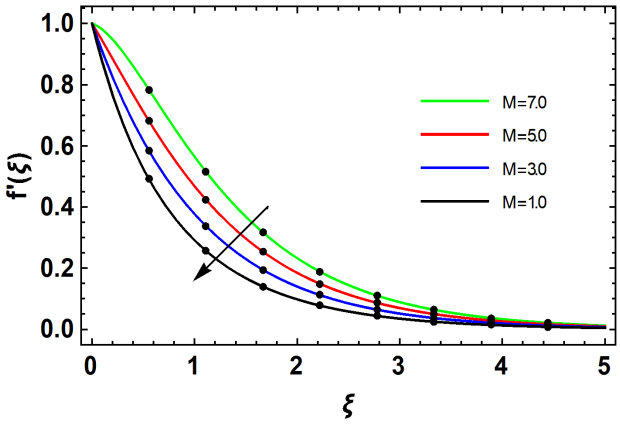

Figure 2. Variation in $f'(\xi)$ via M.

Figures 2 and 3 highlights the effect of the magnetic parameter on velocity profiles $f'(\xi)$ and $g'(\xi)$. From figure it is concluded that the velocity profile decreases with higher values of magnetic parameter. Because the increasing values of the magnetic parameter produce a force which is called the Lorentz force, opposite in direction of motion of the fluid. Therefore, when M increases, the velocity profile decreases. When the magnetic parameter increases, the temperature profile increases. Because magnetic field produces Lorentz force which opposes fluid motion and

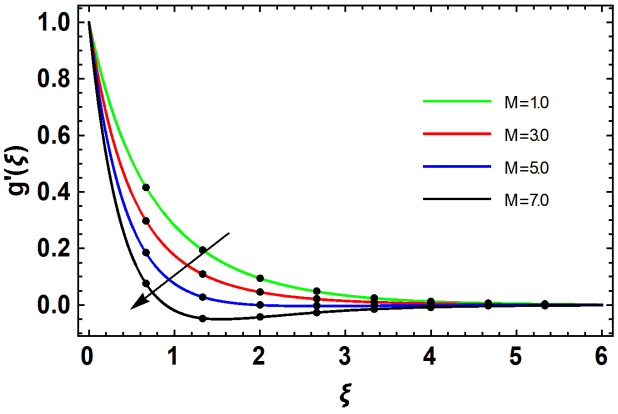

Figure 3. Variation in $g'(\xi)$ via M.

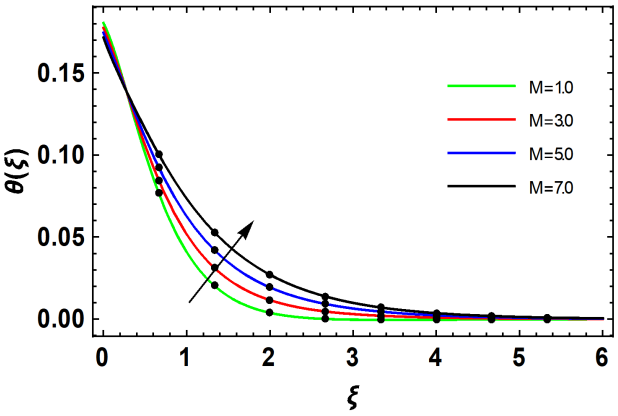

Figure 4. Variation in $\theta(\xi)$ via M.

creates resistance. This resistance leads to higher temperatures. Therefore, when M increases, the temperature profile increases. Figure 4 highlights the effect of M on temperature profile $\theta(\xi)$.

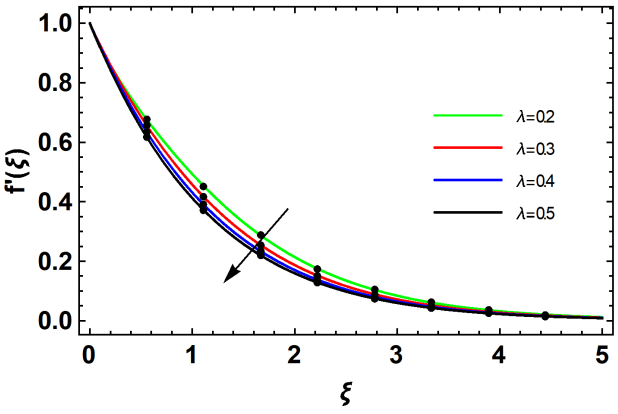

Figure 5. Variation in $f'(\xi)$ via λ.

Figures 5, 6 and 7 highlights the effect of the Casson parameter β on velocity profiles $f'(\xi)$, $g'(\xi)$ and temperature profile $\theta(\xi)$. The velocity field decreases with an increase in the Casson parameter. This implies that the fluid becomes more viscous with a greater Casson parameter β, which lowers the yield stress and momentum inside the boundary layer. Consequently,

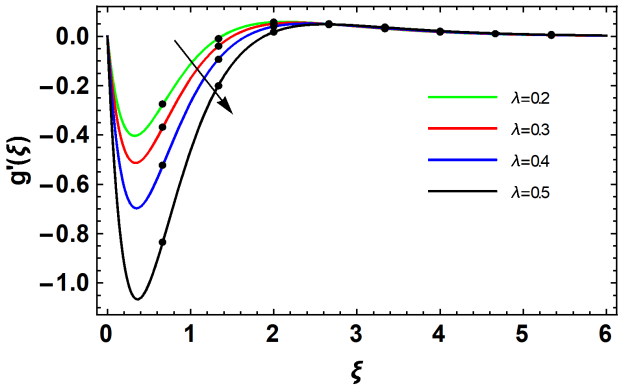

Figure 6. Variation in $g'(\xi)$ via λ.

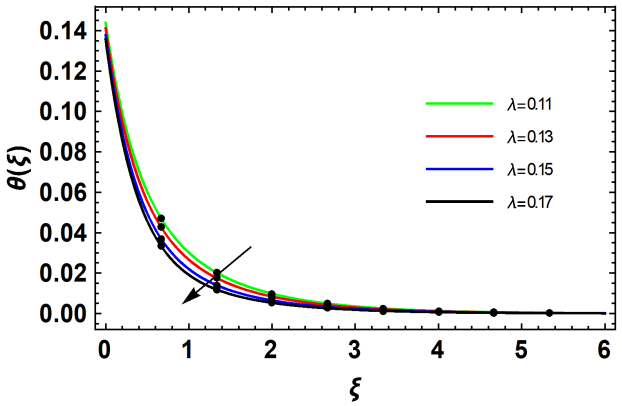

Figure 7. Variation in $\theta(\xi)$ via λ.

when the value of β rises, the velocity profile decreases as the boundary layer thickness decreases. The way that β behaves on $\theta(\xi)$ demonstrates that the fluid temperature drops as β rises. This is explained by the fact that a thinner thermal boundary layer is produced when yield stress is reduced due to a greater β. The fluid's temperature drops as the thermal boundary layer gets thinner.

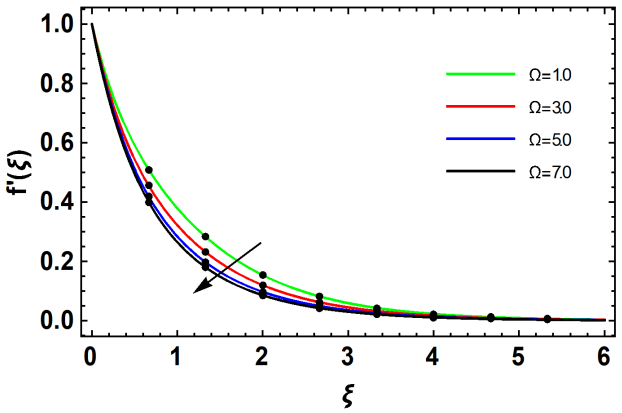

Figure 8. Variation in $f'(\xi)$ via Ω.

The corresponding Figures 8 and 9 demonstrate how the rotational parameter Ω affects the velocity profiles $f'(\xi)$ and $g'(\xi)$. Both velocity profiles

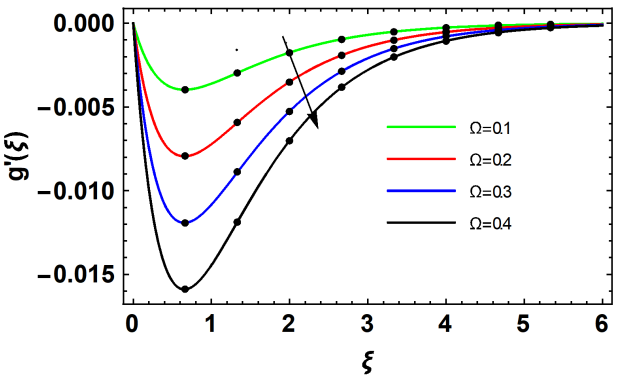

Figure 9. Variation in $g'(\xi)$ via Ω.

noticeably decrease when Ω increases. This happens physically because rotation suppresses the primary and secondary flow velocities by introducing a Coriolis force that acts perpendicular to the flow direction.

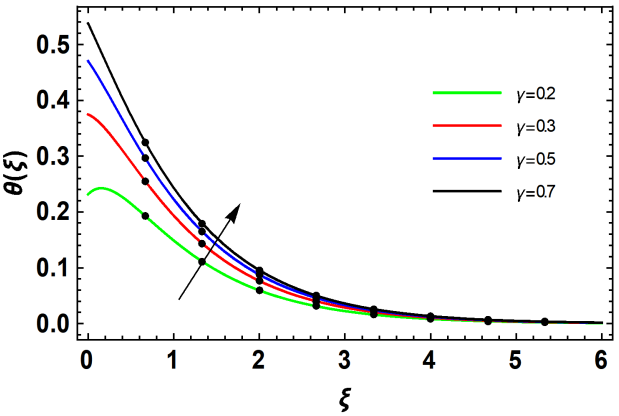

Figure 10. Variation in $\theta(\xi)$ via γ.

For the higher value of parameter γ, the temperature profile $\theta(\xi)$ increases. Figure 10 highlights the effect of γ on temperature profile $\theta(\xi)$. Increasing the thermal Biot number γ usually results in a thicker thermal boundary layer. This is because heat diffusion from the fluid's surface is enhanced by higher convective heat transfer rates, which are associated with larger Biot numbers. As a result, the temperature gradient near the surface decreases, and the thermal boundary layer extends deeper into the fluid.

Figure 11 shows the rise in fluid temperature with the Eckert number Ec. Frictional heating is responsible for this tendency, in which the fluid's increased viscous dissipation produces more thermal energy. The kinetic energy to the enthalpy difference between the fluid and the boundary surface is represented by the Eckert number Ec. Due to viscous factors, more kinetic energy is converted into internal energy as Ec rises, raising the fluid's temperature. As a result, the dimensionless temperature $\theta(\xi)$ increases with a

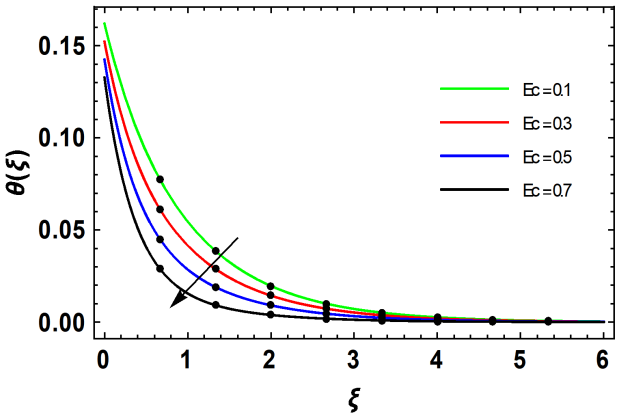

Figure 11. Variation in $\theta(\xi)$ via Ec.

higher Eckert number Ec.

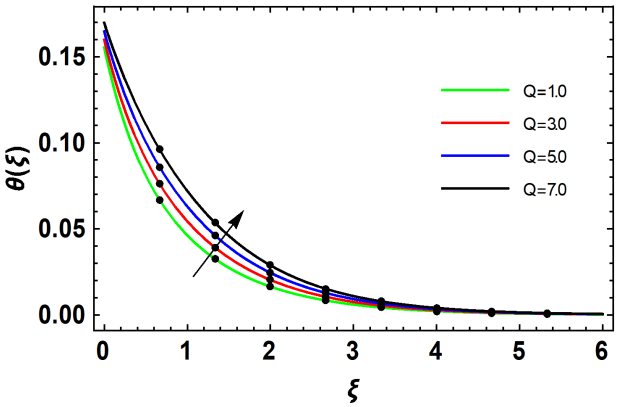

Figure 12. Variation in $\theta(\xi)$ via Q.

The impact of the heat source parameter Q on the temperature distribution $\theta(\xi)$ is depicted in Figure 12. As Q rises, the temperature profile shows an upward trend.

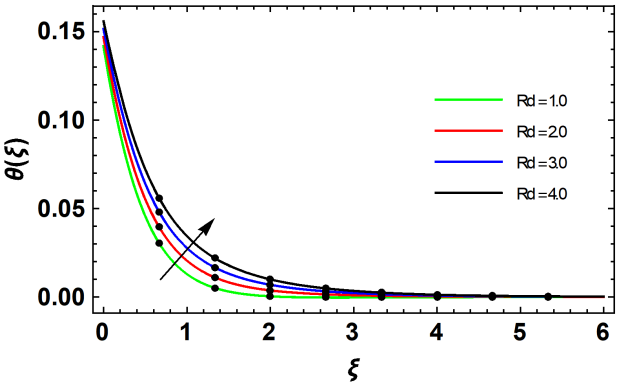

Figure 13. Variation in $\theta(\xi)$ via Rd..

The effect of the thermal radiation parameter R_d on the temperature profile $\theta(\xi)$ is shown in Figure 13. The graph makes it clear that as R_d grows, the temperature rises correspondingly. The thickening of the thermal boundary layer, which is caused by stronger thermal radiation effects at higher values of R_d, is responsible for this improvement in the thermal profile.

Tables 3, 4 and 5 show the effect of $\phi_1, \phi_2, \beta, \Omega, M, R_d$ and Q on skin friction coefficients C_f, C_g and Nusselt number Nu for hybrid nanofluid (Al_2O_3-Cu/kerosene), respectively.

The computed values of the skin friction coefficient $C_f r^{1/2}$ for the Al_2O_3-Cu/kerosene hybrid nanofluid are presented in Table 3. It is observed that as the nanoparticle volume fractions ϕ_{s1} and ϕ_{s2} increase from 0.01 to 0.03, the magnitude of C_f decreases (from -0.198 to -0.184). An increase in the Casson parameter λ (from 0.6 to 0.9) leads to an increase in the magnitude of C_f. The rotation parameter Ω shows a strong decreasing effect on the magnitude of C_f as Ω increases from 0.2 to 0.5. Similarly, the magnetic parameter M slightly reduces the magnitude of C_f with increasing values. In contrast, both the radiation parameter R_d and heat source parameter Q cause an increase in the magnitude of C_f as their values rise.

Table 3. Computed values of the skin friction coefficient C_f for Al_2O_3-Cu/kerosene hybrid nanofluid.

ϕ_{s1}	ϕ_{s2}	λ	Ω	M	R_d	Q	Al_2O_3-Cu/kerosene
0.01	0.01	0.6	0.2	0.1	0.1	1.0	-0.198246
0.02	0.02						-0.192519
0.03	0.03						-0.184477
		0.7					-0.190192
		0.8					-0.198463
		0.9					-0.202453
			0.3				-0.158890
			0.4				-0.146411
			0.5				-0.135737
				0.3			-0.173476
				0.5			-0.173312
				0.7			-0.173169
					0.2		-0.176343
					0.3		-0.180122
					0.4		-0.183451
						3.0	-0.187345
						5.0	-0.190021
						7.0	-0.195532

Table 4 displays the values of the skin friction coefficient $C_g r^{1/2}$. The magnitude of C_g increases with higher nanoparticle volume fractions ϕ_{s1} and ϕ_{s2} (from -0.487 to -0.539). The Casson parameter λ exhibits a non-monotonic behavior, but overall tends to reduce the magnitude in some ranges. Increasing the rotation parameter Ω and magnetic parameter M both lead to a decrease in the magnitude of C_g. The heat source parameter Q shows an increasing effect on the magnitude of C_g as Q rises from 1.0 to 7.0.

Table 4. Computed values of the skin friction coefficient C_g for Al_2O_3-Cu/kerosene hybrid nanofluid.

ϕ_{s1}	ϕ_{s2}	λ	Ω	M	Q	Al_2O_3-Cu/kerosene
0.01	0.01	0.6	0.2	0.1	1.0	-0.486627
0.02	0.02					-0.511967
0.03	0.03					-0.538907
		0.7				-0.868212
		0.8				-0.567374
		0.9				-0.567066
			0.3			-0.522488
			0.4			-0.484038
			0.5			-0.450855
				0.3		-0.533451
				0.5		-0.510266
				0.7		-0.488345
					3.0	-0.476243
					5.0	-0.512832
					7.0	-0.543451

The local Nusselt number $Nur^{-1/2}$ values for the Al_2O_3-Cu/kerosene hybrid nanofluid are shown in Table 5. The results indicate that the Nusselt number increases with increasing nanoparticle volume fractions ϕ_{s1} and ϕ_{s2} (from 0.179 to 0.211), suggesting enhanced heat transfer rate due to the presence of hybrid nanoparticles. Similarly, higher values of the Casson parameter λ, rotation parameter Ω, magnetic parameter M, radiation parameter R_d, and heat source parameter Q all contribute to an increase in the Nusselt number, implying improved convective heat transfer performance under these conditions.

Table 5. Computed values of the Nusselt number Nu for Al_2O_3-Cu/kerosene hybrid nanofluid.

ϕ_{s1}	ϕ_{s2}	λ	Ω	M	R_d	Q	Al_2O_3-Cu/kerosene
0.01	0.01	0.6	0.2	0.1	0.1	1.0	0.179427
0.02	0.02						0.194138
0.03	0.03						0.211145
		0.7					0.190192
		0.8					0.198993
		0.9					0.209453
			0.3				0.158899
			0.4				0.178854
			0.5				0.199847
				0.3			0.173476
				0.5			0.177653
				0.7			0.180021
					0.2		0.176343
					0.3		0.180122
					0.4		0.183651
						3.0	0.182345
						5.0	0.190121
						7.0	0.195512

6 Conclusion

In conclusion, the three-dimensional magnetohydrodynamics (MHD) radiative flow of a hybrid nanofluid over a stretching sheet was thoroughly investigated in this study using the homotopy analysis method, which yielded important insights into the intricate interactions between the physical parameters controlling such systems. The work demonstrated the strong influence of important variables, such as rotation parameter, biot number, and magnetic field strength, on the temperature and velocity distributions inside the nanofluid flow by deriving convergent series solutions. The results show that adjusting these factors can dramatically change the thermal properties and flow dynamics, providing a technique to maximize heat transfer in cutting-edge engineering applications. In addition to improving theoretical knowledge of hybrid nanofluid behavior under the influence of radiative and magnetic forces, the methodology used in this work creates a strong analytical foundation for forecasting and managing thermal performance in real-world scenarios. Furthermore, the results indicate that more research into the application of various nanoparticle combinations, different base fluids, and different flow configurations may increase the usefulness and effectiveness of hybrid nanofluids in technological and industrial processes, opening the door for further advancements in energy systems and thermal management.

Data Availability Statement

Data will be made available on request.

Funding

This work was supported without any funding.

Conflicts of Interest

The authors declare no conflicts of interest.

AI Use Statement

The authors declare that no generative AI was used in the preparation of this manuscript.

Ethical Approval and Consent to Participate

Not applicable.

References

[1] Taylor, R., Coulombe, S., Otanicar, T., Phelan, P., Gunawan, A., Lv, W., ... & Tyagi, H. (2013). Small particles, big impacts: A review of the diverse applications of nanofluids. *Journal of applied physics, 113*(1), 011301. [CrossRef]

[2] Buongiorno, J. (2006). Convective Transport in Nanofluids. *Journal of Heat Transfer, 128*(3), 240-250. [CrossRef]

[3] Banisharif, A., Estellé, P., Rashidi, A., Van Vaerenbergh, S., & Aghajani, M. (2021). Heat transfer properties of metal, metal oxides, and carbon water-based nanofluids in the ethanol condensation process. *Colloids and Surfaces A: Physicochemical and Engineering Aspects, 622*, 126720. [CrossRef]

[4] Minkowycz, W. J., Sparrow, E., & Abraham, J. P. (Eds.). (2016). *Nanoparticle heat transfer and fluid flow*. CRC press.

[5] Das, S. K., Choi, S. U. S., Yu, W., & Pradeep, T. (2007). *Nanofluids: Science and Technology*. Wiley-Interscience.

[6] Kakaç, S., & Pramuanjaroenkij, A. (2009). Review of convective heat transfer enhancement with nanofluids. *International journal of heat and mass transfer, 52*(13-14), 3187-3196. [CrossRef]

[7] Witharana, S., Chen, H., & Ding, Y. (2011). Stability of nanofluids in quiescent and shear flow fields. *Nanoscale Research Letters, 6*(1), 231. [CrossRef]

[8] Chen, H., Witharana, S., Jin, Y., Kim, C., & Ding, Y. (2009). Predicting thermal conductivity of liquid suspensions of nanoparticles (nanofluids) based on rheology. *Particuology, 7*(2), 151-157. [CrossRef]

[9] Mahian, O., Kolsi, L., Amani, M., Estellé, P., Ahmadi, G., Kleinstreuer, C., ... & Pop, I. (2019). Recent advances in modeling and simulation of nanofluid flows-Part I: Fundamentals and theory. *Physics reports, 790*, 1-48. [CrossRef]

[10] Sreekumar, S., Shah, N., Mondol, J. D., Hewitt, N., & Chakrabarti, S. (2022). Numerical investigation and feasibility study on MXene/water nanofluid based photovoltaic/thermal system. *Cleaner Energy Systems, 2*, 100010. [CrossRef]

[11] Alizadeh, M. R., & Dehghan, A. A. (2014). Conjugate natural convection of nanofluids in an enclosure with a volumetric heat source. *Arabian Journal for Science and Engineering, 39*(2), 1195-1207. [CrossRef]

[12] Maiga, S. E. B., Palm, S. J., Nguyen, C. T., Roy, G., & Galanis, N. (2005). Heat transfer enhancement by using nanofluids in forced convection flows. *International journal of heat and fluid flow, 26*(4), 530-546. [CrossRef]

[13] Kuznetsov, A. V., & Nield, D. A. (2010). Natural convective boundary-layer flow of a nanofluid past a vertical plate. *International Journal of Thermal Sciences, 49*(2), 243-247. [CrossRef]

[14] Wasan, D. T., & Nikolov, A. D. (2003). Spreading of nanofluids on solids. *Nature, 423*(6936), 156-159. [CrossRef]

[15] Kuntoglu, M. (2022). State of the Art on Hybrid Nanofluids and Their Usage in Machining Processes. *Nanomaterials in Manufacturing Processes*, 1-30.

[16] Abbasi, S., Zebarjad, S. M., Baghban, S. H. N., Youssefi, A., & Ekrami-Kakhki, M. S. (2016). Experimental investigation of the rheological behavior and viscosity of decorated multi-walled carbon nanotubes with TiO2 nanoparticles/water nanofluids. *Journal of Thermal Analysis and Calorimetry, 123*(1), 81-89. [CrossRef]

[17] Barbés, B., Páramo, R., Blanco, E., & Casanova, C. (2014). Thermal conductivity and specific heat capacity measurements of CuO nanofluids. *Journal of Thermal Analysis and Calorimetry, 115*(2), 1883-1891. [CrossRef]

[18] Shamshirband, S., Malvandi, A., Karimipour, A., Goodarzi, M., Afrand, M., Petković, D., ... & Mahmoodian, N. (2015). Performance investigation of micro-and nano-sized particle erosion in a 90 elbow using an ANFIS model. *Powder Technology, 284*, 336-343. [CrossRef]

[19] Hemmat Esfe, M., Saedodin, S., Yan, W. M., Afrand, M., & Sina, N. (2016). Study on thermal conductivity of water-based nanofluids with hybrid suspensions of CNTs/Al2O3 nanoparticles. *Journal of Thermal Analysis and Calorimetry, 124*(1), 455-460. [CrossRef]

[20] Choi, S. U. (1995, November). Enhancing thermal conductivity of fluids with nanoparticles. In *ASME international mechanical engineering congress and exposition* (Vol. 17421, pp. 99-105). American Society of Mechanical Engineers. [CrossRef]

[21] Kang, H. U., Kim, S. H., & Oh, J. M. (2006). Estimation of thermal conductivity of nanofluid using experimental effective particle volume. *Experimental Heat Transfer, 19*(3), 181-191. [CrossRef]

[22] Lee, S., Eastman, J. A., Li, S. A., & Choi, S. S. (1999). Measuring thermal conductivity of fluids containing oxide nanoparticles. *Journal of Heat Transfer, 121*(2), 280-289. [CrossRef]

[23] Eastman, J. A., Choi, S. U. S., Li, S., Yu, W., & Thompson, L. J. (2001). Abnormally elevated effective heat conductivities of copper nanoparticle-containing ethylene glycol-based nanofluids. *Applied Physics Letters, 78*, 718-720. [CrossRef]

[24] Aybar, H. Ş., Sharifpur, M., Azizian, M. R., Mehrabi, M., & Meyer, J. P. (2015). A review of thermal conductivity models for nanofluids. *Heat Transfer Engineering, 36*(13), 1085-1110. [CrossRef]

[25] Ahmed, N., Khan, U., & Mohyud-Din, S. T. (2017). The impact of an effective Prandtl number model on the squeezed flow of γAl2O3-H2O and γAl2O3-C2H6O2 nanofluids was examined. *Journal of Molecular Liquids, 238*, 447-454. [CrossRef]

[26] Sun, B., Yang, D., Li, H., & Guo, Y. (2020). The

impact of a continuous magnetic field on Fe3O4/water magnetic convective heat transfer nanofluid in circular, horizontal tubes. *Applied Thermal Engineering, 171*, 114920. [CrossRef]

[27] Kumar, P. M., & Kumar, C. A. (2020). Al2O3/water nanofluids are used in a numerical analysis of the heat transfer performance of an electronic chip's six circular channel heat sink. *Materials Today: Proceedings, 21*, 194-201. [CrossRef]

[28] Lahmar, S., Kezzar, M., Eid, M. R., & Sari, M. R. (2020). Heat transfer of squeezing unsteady nanofluid flow under the effects of an inclined magnetic field and variable thermal conductivity. *Physica A: Statistical Mechanics and Its Applications, 540*, 123138. [CrossRef]

[29] Sheikholeslami, M., & Rokni, H. B. (2018). Numerical simulation for impact of Coulomb force on nanofluid heat transfer in a porous enclosure in presence of thermal radiation. *International Journal of Heat and Mass Transfer, 118*, 823-831. [CrossRef]

[30] Gbadeyan, J. A., Titiloye, E. O., & Adeosun, A. T. (2020). Effect of changing thermal conductivity and viscosity on Casson nanofluid flow with convective heating and velocity slip. *Heliyon, 6*, e03076. [CrossRef]

[31] Fedele, L., Colla, L., & Bobbo, S. (2012). Viscosity and thermal conductivity measurements of water-based nanofluids containing titanium oxide nanoparticles. *International journal of refrigeration, 35*(5), 1359-1366. [CrossRef]

[32] Gulzar, O., Qayoum, A., & Gupta, R. (2019). Experimental study on stability and rheological behaviour of hybrid Al2O3-TiO2 Therminol-55 nanofluids for concentrating solar collectors. *Powder Technology, 352*, 436-444. [CrossRef]

[33] Sarkar, J., Ghosh, P., & Adil, A. (2015). A review on hybrid nanofluids: recent research, development and applications. *Renewable and Sustainable Energy Reviews, 43*, 164-177. [CrossRef]

[34] Yang, L., Ji, W., Mao, M., & Huang, J. N. (2020). Dynamic stability, sedimentation, and time-dependent heat transfer characteristics of TiO2 and CNT nanofluids. *Journal of Thermal Analysis and Calorimetry, 141*(3), 1183-1195. [CrossRef]

[35] Khashi'ie, N. S., Arifin, N. M., Nazar, R., Hafidzuddin, E. H., Wahi, N., & Pop, I. (2020). Magnetohydrodynamics (MHD) axisymmetric flow and heat transfer of a hybrid nanofluid past a radially permeable stretching/shrinking sheet with Joule heating. *Chinese Journal of Physics, 64*, 251-263. [CrossRef]

[36] Wole-Osho, I., Okonkwo, E. C., Kavaz, D., & Abbasoglu, S. (2020). An experimental investigation into the effect of particle mixture ratio on specific heat capacity and dynamic viscosity of Al2O3-ZnO hybrid nanofluids. *Powder Technology, 363*, 699-716. [CrossRef]

[37] Aly, E. H., & Pop, I. (2020). MHD flow and heat transfer near stagnation point over a stretching/shrinking surface with partial slip and viscous dissipation: hybrid nanofluid versus nanofluid. *Powder Technology, 367*, 192-205. [CrossRef]

[38] Aghahadi, M. H., Niknejadi, M., & Toghraie, D. (2019). An experimental study on the rheological behavior of hybrid Tungsten oxide (WO3)-MWCNTs/engine oil Newtonian nanofluids. *Journal of Molecular Structure, 1197*, 497-507. [CrossRef]

[39] Hayat, T., Aziz, A., Muhammad, T., & Alsaedi, A. (2018). Darcy-Forchheimer flow of nanofluid in a rotating frame. *International Journal of Numerical Methods for Heat & Fluid Flow, 28*(12), 2895-2915. [CrossRef]

[40] Huminic, G., & Huminic, A. (2020). Entropy formation of nanofluid and hybrid nanofluid flow in thermal systems: a review. *Journal of Molecular Liquids, 302*, 112533. [CrossRef]

[41] Huminic, G., & Huminic, A. (2018). Heat transfer capability of the hybrid nanofluids for heat transfer applications. *Journal of Molecular Liquids, 272*, 857-870. [CrossRef]

[42] Saba, F., Ahmed, N., Khan, U., & Mohyud-Din, S. T. (2019). A novel coupling of (CNT-Fe3O4/H2O) hybrid nanofluid for improvements in heat transfer for flow in an asymmetric channel with dilating/squeezing walls. *International Journal of Heat and Mass Transfer, 136*, 186-195. [CrossRef]

[43] de Oliveira, L. R., Ribeiro, S. R. F. L., Reis, M. H. M., Cardoso, V. L., & Bandarra Filho, E. P. (2019). Experimental study on the thermal conductivity and viscosity of ethylene glycol-based nanofluid containing diamond-silver hybrid material. *Diamond and Related Materials, 96*, 216-230. [CrossRef]

[44] Iqbal, Z., Akbar, N. S., Azhar, E., & Maraj, E. N. (2018). Performance of hybrid nanofluid (Cu-CuO/water) on MHD rotating transport in oscillating vertical channel inspired by Hall current and thermal radiation. *Alexandria engineering journal, 57*(3), 1943-1954. [CrossRef]

[45] Rahimi-Gorji, M., Pourmehran, O., Hatami, M., & Ganji, D. D. (2015). Statistical optimization of microchannel heat sink (MCHS) geometry cooled by different nanofluids using RSM analysis. *The European Physical Journal Plus, 130*(2), 22. [CrossRef]

[46] Pourmehran, O., Rahimi-Gorji, M., Hatami, M., Sahebi, S. A. R., & Domairry, G. (2015). Numerical optimization of microchannel heat sink (MCHS) performance cooled by KKL based nanofluids in saturated porous medium. *Journal of the Taiwan Institute of Chemical Engineers, 55*, 49-68. [CrossRef]

[47] Gupta, M., Arora, N., Kumar, R., Kumar, S., & Dilbaghi, N. (2014). A comprehensive review of experimental investigations of forced convective heat transfer characteristics for various nanofluids. *International journal of mechanical and materials engineering, 9*(1), 11.

[CrossRef]

[48] Safaei, M. R., Safdari Shadloo, M., Goodarzi, M. S., Hadjadj, A., Goshayeshi, H. R., Afrand, M., & Kazi, S. N. (2016). A survey on experimental and numerical studies of convection heat transfer of nanofluids inside closed conduits. *Advances in Mechanical Engineering, 8*(10), 1687814016673569. [CrossRef]

[49] Wu, J. M., & Zhao, J. (2013). A review of nanofluid heat transfer and critical heat flux enhancement—research gap to engineering application. *Progress in Nuclear Energy, 66*, 13-24. [CrossRef]

[50] Wong, K. V., & Castillo, M. J. (2010). Heat transfer mechanisms and clustering in nanofluids. *Advances in Mechanical Engineering, 2*, 795478. [CrossRef]

[51] Rudyak, V. Y., Minakov, A. V., & Krasnolutskii, S. L. (2016). Physics and mechanics of heat exchange processes in nanofluid flows. *Physical mesomechanics, 19*(3), 298-306. [CrossRef]

[52] Mohammed, H. A., Bhaskaran, G., Shuaib, N. H., & Saidur, R. (2011). Heat transfer and fluid flow characteristics in microchannels heat exchanger using nanofluids: a review. *Renewable and Sustainable Energy Reviews, 15*(3), 1502-1512. [CrossRef]

[53] Tabasum, R., Mehmood, R., & Pourmehran, O. (2018). Velocity slip in mixed convective oblique transport of titanium oxide/water (nano-polymer) with temperature-dependent viscosity. *The European Physical Journal Plus, 133*(9), 361. [CrossRef]

[54] Alfvén, H. (1942). Existence of Electromagnetic-Hydrodynamic Waves. *Nature, 150*(3805), 405-406. [CrossRef]

[55] Alfvén, H. (1943). On the Existence of Electromagnetic-Hydrodynamic Waves. *Arkiv för matematik, astronomi och fysik, 29B*(2), 1-7.

[56] Roberts, P. H., & King, E. M. (2013). On the genesis of the Earth's magnetism. *Reports on Progress in Physics, 76*(9), 096801. [CrossRef]

[57] Christensen, U. R. (2010). Dynamo scaling laws and applications to the planets. *Space science reviews, 152*(1), 565-590. [CrossRef]

[58] Glatzmaiers, G. A., & Roberts, P. H. (1995). A three-dimensional self-consistent computer simulation of a geomagnetic field reversal. *Nature, 377*(6546), 203-209. [CrossRef]

[59] Jones, C. A. (2011). Planetary magnetic fields and fluid dynamos. *Annual Review of Fluid Mechanics, 43*(1), 583-614. [CrossRef]

[60] Sheikholeslami, M., Ganji, D. D., Gorji-Bandpy, M., & Soleimani, S. (2014). Magnetic field effect on nanofluid flow and heat transfer using KKL model. *Journal of the Taiwan Institute of Chemical Engineers, 45*(3), 795-807. [CrossRef]

[61] Naramgari, S., & Sulochana, C. (2016). MHD flow over a permeable stretching/shrinking sheet of a nanofluid with suction/injection. *Alexandria Engineering Journal, 55*(2), 819-827. [CrossRef]

[62] Howell, J. R., Mengüç, M. P., Daun, K., & Siegel, R. (2020). *Thermal radiation heat transfer*. CRC press.

[63] Meseguer, J., Pérez-Grande, I., & Sanz-Andrés, A. (2012). *Spacecraft thermal control*. Elsevier.

[64] Planck, M. (1914). *The Theory of Heat Radiation*. P Blakiston's Son & Co.

[65] Huang, K. (2008). *Statistical mechanics*. John Wiley & Sons.

[66] Liao, S. J. (1992). *The proposed homotopy analysis technique for the solution of nonlinear problems* (Doctoral dissertation, Ph. D. Thesis, Shanghai Jiao Tong University).

[67] Liao, S. J. (1999). An explicit, totally analytic approximation of Blasius' viscous flow problems. *International Journal of Non-Linear Mechanics, 34*(4), 759-778. [CrossRef]

[68] Liao, S. (2003). *Beyond perturbation: introduction to the homotopy analysis method*. Chapman and Hall/CRC.